ACS APPLIED MATERIALS & INTERFACES

Research Article

www.acsami.org

Polarization-Control of the Potential Barrier at the Electrode Interfaces in Epitaxial Ferroelectric Thin Films

Ioana Pintilie, Cristian Mihail Teodorescu, Corneliu Ghica, Cristina Chirila, Andra Georgia Boni, Luminita Hrib, Iuliana Pasuk, Raluca Negrea, Nicoleta Apostol, and Lucian Pintilie*

National Institute of Materials Physics, Atomistilor 105 bis, Magurele 077125, Romania

Supporting Information

ABSTRACT: Electrode interface is a key element in controlling the macroscopic electrical properties of the ferroelectric capacitors based on thin films. In the case of epitaxial ferroelectrics, the electrode interface is essential in controlling the leakage current and the polarization switching, two important elements in the read/write processes of nonvolatile memories. However, the relation between the polarization bound charges and the electronic properties of the electrode interfaces is not yet well understood. Here we show that polarization charges are controlling the height of the potential barriers at the electrode interfaces in the case of $Pb(Zr,Ti)O_3$ and $BaTiO_3$ epitaxial films. The results suggest that the height is set to a value allowing rapid compensation of the depolarization field during the polarization switching, being almost independent of the metals used for electrodes. This general behavior open a new perspective in engineering interface properties and designing new devices based on epitaxial ferroelectrics.

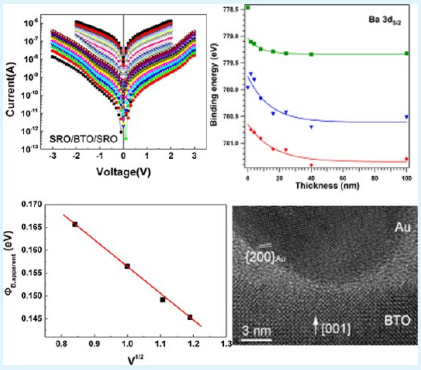

KEYWORDS: *ferroelectric, electrode interface, potential barrier, leakage current, hysteresis, capacitance*

1. INTRODUCTION

Ferroelectric materials are used in nonvolatile memories, as well as in other applications, under the form of capacitors.[1,2] The metal−ferroelectric−metal (MFM) structure thus includes the two electrode−ferroelectric interfaces, which can have a significant impact on the macroscopic electrical properties, as shown in recent studies.[3−8] Although it is accepted that the electrode interface may have influence on some of the specific quantities of the MFM structures such as polarization value, dielectric constant (dead layer models), leakage current, or the generated photovoltage, quite a few efforts have been dedicated to finding out if there is a connection between the bound polarization charges located near the interface and the electronic properties of the interface (e.g., the height of the potential barrier).[9−13] Only recently it was shown that the band bending at the electrode interface is dependent on the polarization orientation.[14,15] Also, the height of the Schottky-type potential barrier at the electrode−ferroelectric interface was determined from XPS studies, with values well above 1 eV both for electrons and holes.[16−18] However, these results do not agree with the values obtained from the macroscopic current−voltage (I−V) measurements, which are considerably lower than the one determined from XPS investigations (in the 0.2−0.8 eV range).[19−21]

Understanding the formation of the electrode interface and the relation between the polarization charges and the electronic properties of the interface is critical in controlling the polarization switching and the magnitude of the leakage current. These two are important elements in the read/write processes in nonvolatile memories.[2] The relation between polarization and electrode interface is better studied using good quality epitaxial ferroelectrics, avoiding in this way the deleterious effects of the grain boundaries (large extrinsic contribution to the dielectric constant, back-switching effect, low carrier mobility, etc.).[22−24] In the ferroelectric capacitors based on high-quality epitaxial films the hysteresis loop is rectangular.[25] This can be attributed to the absence of the pinning centers for the ferroelectric domains, associated with grain boundaries, but also to a very efficient mechanism for the screening of the depolarization field during the switching process. The last one may be related to the height of the potential barriers at the electrode interfaces, which seems to be influenced by the magnitude and orientation of the ferroelectric polarization.[26−28]

Here we show that the ferroelectric polarization is actually controlling the height of the potential barrier in the case of epitaxial lead zirconate-titanate (PZT) and $BaTiO_3$ (BTO) thin films. This is happening around room temperature and on a limited voltage range, where the work function difference between the metal electrode and the ferroelectric seems to not count in the height of the potential barrier. The estimated values from I−V measurements are low in general, between 0.1 and 0.3 eV for both ferroelectric materials. Tentatively it is assumed that the polarization charges set the potential barriers to heights allowing rapid compensation of the depolarization field during the switching process, leading to rectangular

Received: December 2, 2013
Accepted: January 21, 2014
Published: January 21, 2014

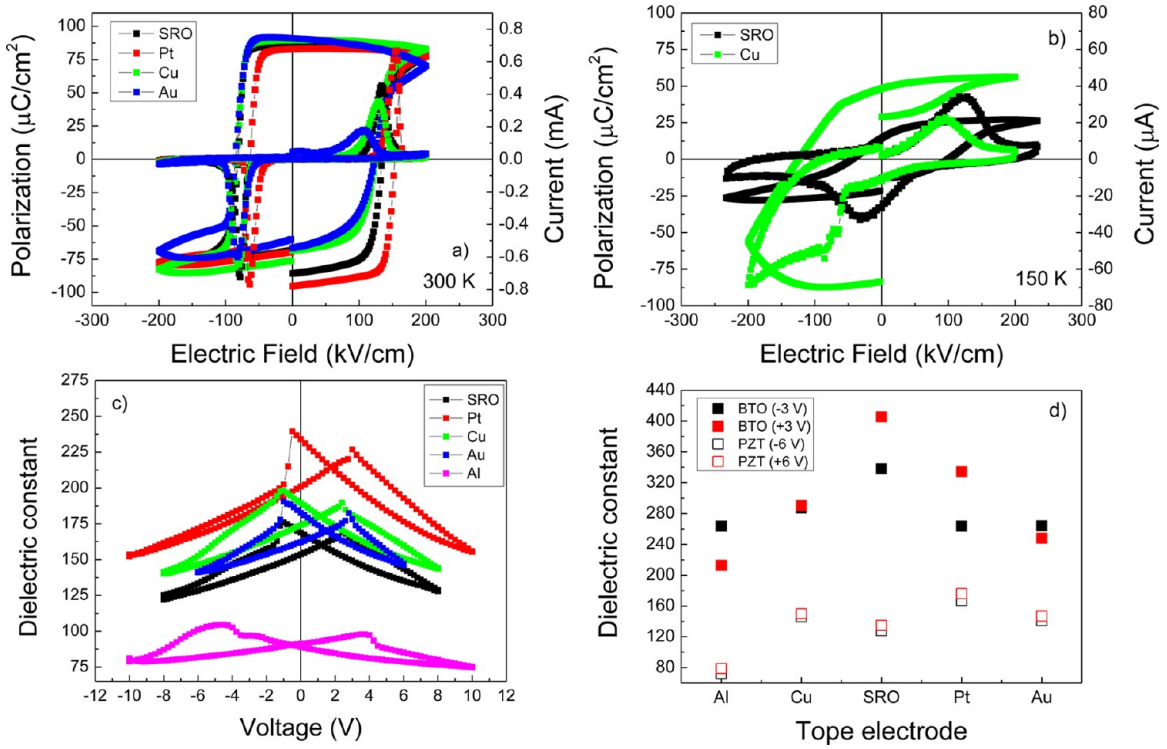

Figure 1. (a) Hysteresis loops, at room temperature, for PZT layer with top Cu, Au, Pt, and SRO as top contacts; (b) hysteresis loops at 150 K for BTO layer with top SRO and Cu contacts; (c) $C-V$ characteristics for PZT with top Cu, Au, Pt, SRO, and Al contacts; (d) dielectric constants, for different top metal electrodes, calculated from the capacitance measured at voltages where the ferroelectric polarization is saturated. In the Supporting Information can be found hysteresis loops for other top metals, the procedure for the estimation of the ferroelectric polarization from the current hysteresis in the case of BTO layer (eliminating the leakage contribution) and $C-V$ characteristics for the BTO.

hysteresis loops and sharp peaks in the capacitance−voltage ($C-V$) measurements. The microscopic analysis performed by X-ray photoelectron spectroscopy (XPS) and by high resolution transmission electron microscopy (HR-TEM) reveals interesting facts regarding the formation of the electrode-ferroelectric interface such as the Fermi level position, structure of the metal electrode, band-bending at the interface, etc. The image emerging from this study is that the epitaxial ferroelectric capacitor is almost intrinsic in the bulk and has the bound polarization charges and the compensation charges located in thin regions near electrode interfaces. The results of our study can be considered as an experimental evidence of the interface theorem stating that insulating interfaces are required to see a polarization difference as an interface charge.[29,30]

3. EXPERIMENTAL SECTION

Growth of the Films. The method used for the growth of the films was pulsed laser deposition (PLD) using a KrF laser (wavelength 248 nm, 700 mJ energy, and 10 Hz repetition rate), in a deposition chamber foreseen with a 4 targets carrousel and a substrate holder that can be heated up to 1000 °C. The depositions were performed on single-crystal $SrTiO_3$ (STO) substrates with (001) orientation, with a miscut angle of lower than 0.50. To obtain epitaxial PZT films, the surface of the STO (100) substrate was cleaned in hydrofluoric acid (HF) buffer solution and then annealed in air at 1000 °C for 2 h. Smooth terraces of one unit cell step were obtained in this way. A SRO epitaxial buffer layer with a thickness of around 20 nm has been deposited on STO, this acting as a bottom electrode and also as an excellent template for the heteroepitaxial growth of high-quality ferroelectric perovskites. The bottom electrode was deposited at a substrate temperature of 700 °C, in a background atmosphere of 0.133 mbar oxygen, with a laser fluence of 2 J/cm^2 and a repetition rate of 5 Hz. The PZT ferroelectric thin film with Zr/Ti ratio of 20/80 was deposited at 575 °C, 0.2 mbar oxygen atmosphere, with a laser fluence of 2 J/cm^2 and a repetition rate of 5 Hz. After deposition the BTO layer was annealed at 575 °C in oxygen atmosphere at 1 bar, for 1 h, to compensate the oxygen vacancies. The BTO ferroelectric layer was deposited at 700 °C, 0.14 mbar oxygen atmosphere, with a laser fluence of 1.5 J/cm^2 and a repetition rate of 5 Hz. After deposition the PZT layer was annealed at 700 °C in oxygen atmosphere at 1 bar, for 1 h, to compensate the oxygen vacancies.

Fabrication of the MFM Structures. Several metals were used as top electrodes for electrical measurements, namely SRO, Pt, Cu, Au, and Al. The SRO was deposited by PLD at room temperature, while Pt, Cu, Au and Al were deposited by radio frequency (RF) sputtering. The deposition was performed through a shadow mask leaving contacts with area of 100 × 100 μm^2. One has to mention that a mild etching at about 200 °C for 15 min was used prior the metal deposition in order to remove the possible contaminant layer existing on the surface. The purpose was to have an as clean as possible surface. Evaporated electrodes processed in the same conditions as for XPS experiments (see below) were tested but these proved to have a very poor adherence to the ferroelectric layer, making them unsuitable for electrical measurements (see TEM image S19 in the Supporting Information).

Electrical Measurements. A complex setup was used for measurements, comprising off: a Lakeshore cryoprober model CPX-VF, a Keithley electrometer model 6517 (for $I-V$ characteristics), a ferroelectric tester model TF2000 from aixACCT (for hysteresis loops), and an impedance analyzer model HP 4194A (for C−V and C-f characteristics). Hysteresis measurements were performed using a triangular voltage wave with 1 kHz frequency. The C−V measurements were performed using an a.c. small signal of 0.1 V amplitude and 100 kHz frequency. $I-V$ measurements were performed using hysteresis type measurements (zero-(+V_{max})-zero-(−V_{max})-zero). Only the sweeping down part from V_{max} to zero was considered for estimating the potential barriers because this did not contain a parasitic contribution from polarization switching.[31]

Structural characterization. The crystal structure and epitaxial relationships were investigated by high resolution X-ray diffraction (HR-XRD) using a Bruker D8 Advance diffractometer in parallel beam setting. The measurements were performed in coplanar geometry with horizontal sample stage, using monochromatized Cu−Kα1 radiation (λ = 1.5406 Å). High-resolution transmission electron microscopy (HR-TEM) analysis was also performed to evaluate the epitaxial quality of the films deposited on STO substrate and to investigate the electrode−ferroelectric interfaces at microscopic level. The investigations were performed with a model JEM-ARM200F microscope from JEOL.

XPS Investigations. X-ray photoelectron spectroscopy was performed in an analysis chamber (Specs GmbH, Germany) by using a monochromatized Al Kα1 X-ray source (1486.74 eV) with 350 W anode power. Electrons are analyzed by a 150 mm radius Phoibos electron analyzer operating in large area mode with pass energy of 30 eV, in normal emission. The estimated overall energy resolution (Ag $3d_{5/2}$ level on a sputter-annealed foil) in these conditions is of ~0.85 eV total full width at half-maximum (fwhm), including the experimental broadening of the energy analyzer and core hole lifetimes. A flood gun with acceleration voltage of 1 eV and electron current of 0.1 mA was employed to ensure the sample neutralization. Several test experiments were performed before starting the real experiment by varying the X-ray power and the flood gun parameters, in order to identify a region of the parameter space where reproducible binding energies are obtained (i.e., where the charging effects are fully compensated), by taking as a guideline the C 1s energy of inherent contaminants, which must be obtained at 284.60 ± 0.05 eV.

Au, Pt and Cu were deposited at room temperature, close to normal incidence, in a molecular beam epitaxy (MBE) chamber (Specs), in vacuum connected to the analysis chamber (forming altogether a surface science cluster), from a properly outgassed Knudsen cell at a rate of 2.7 ± 0.2 Å/min., as calibrated with a quartz thickness monitor. In the following, we shall refer these thicknesses as "nominal coverages", with respect to the bulk metals, whose parameters were used in the electronics of the thickness monitor during the calibration procedure. All ultrahigh vacuum chambers operate in low 1×10^{-10} mbar vacuum range. The pressure during Au or Cu evaporation was also in the 1×10^{-10} mbar vacuum range.

3. RESULTS AND DISCUSSIONS

The samples were grown by pulsed laser deposition (PLD) on single-crystalline $SrTiO_3$ (001) oriented substrates with a buffer layer of $SrRuO_3$ (SRO) as bottom electrode. The structural quality of the ferroelectric films was investigated by X-ray diffraction (XRD) and HR-TEM. Both methods proved the epitaxial quality of the bottom SRO electrode and of the ferroelectric layer (see Figures S1 and S3 in the Supporting Information). The thickness of the PZT and BTO films was of 300 nm as estimated from HR-TEM. Several materials were used as top contacts on the same ferroelectric film (see Figure S2 in the Supporting Information): two metals with different work functions (Φ) but with the same electronic configuration on the d shell (Au, Φ_{Au} = 5.1 eV;[32] Cu, Φ_{Cu} = 4.65 eV[32]), a metal without d-shell (Al, Φ_{Al} = 4.3 eV[32]), a metal with incomplete d-shell and large workfunction (Pt, Φ_{Pt} = 5.65 eV[32]), and one conductive oxide (SRO, Φ_{SRO} = 4.7−4.9 eV[33]). In all cases, the area of the top contact was of 100×100 μm^2.

3.1. Electrical Measurements. The macroscopic electric measurements included hysteresis loop ($P-E$), capacitance−voltage ($C-V$) and current−voltage ($I-V$) characteristics. Examples of hysteresis loops and C−V characteristics are shown in Figure 1 (see also Figures S4−S9 from the Supporting Information). It was found that: the polarization values are about 90 $\mu C/cm^2$ for PZT and about 25 $\mu C/cm^2$ for BTO; the coercive voltage is about 1.5 V at room temperature for BTO, and about 3 V for PZT; the values for the dielectric constant are about two times larger for BTO compared to PZT. During the hysteresis measurements at room temperature, it was observed that the leakage current is significantly larger in BTO compared to PZT, inflating the loop (see Figure S5 in the Supporting Information). Therefore, measurements for BTO were repeated at lower temperatures, with better results for the current hysteresis although the leakage contribution remains important (see Figure 1b, with details in the Supporting Information). The values of the dielectric constant shown in Figure 1d were calculated from the capacitance measured at a voltage outside the switching range for the polarization, where this is assumed to be saturated according to the hysteresis loops shown in panels a and b in Figure 1.

The hysteresis measurements reveal the fact that the polarization value is about the same, being independent of the material used as top contact. This is an expected result considering that the ferroelectric polarization is a property of the ferroelectric film and should not depend on the metals used as electrodes. Only the contribution of the leakage current to the hysteresis loop seems to be dependent on the top electrode. In the case of the PZT (see Figure 1a) the loops present similar shapes and shifts along the voltage axis. The last result suggests the presence of an internal electric field whose direction points toward the top electrode (upward polarization) and does not change with the metal used for the top contact. This is contradictory with the fact that Au and Pt have work functions (Au, 5.1 eV; Pt, 5.65 eV[32]) higher than SRO (4.7−4.9 eV, dependent on the oxygen content[33]), whereas Cu has a work function (4.65 eV[32]) slightly lower than SRO. If the internal electric field were given only by the work function difference between the top and bottom electrodes, then it should have changed its orientation when Cu is replaced with Au or Pt as top contact. Therefore, the internal electric field has other origins, such as stress gradient, or a gradient in the oxygen content from the bottom electrode interface to the top one, as suggested by preliminary scanning TEM (STEM) studies performed on the cross-section of the ferroelectric layer (see the Supporting Information, last paragraph).

As mentioned above, in the case of BTO the hysteresis loops at room temperature are severely affected by the leakage current on the negative polarity, except the case of the symmetric SRO-BTO-SRO structure. Better hysteresis loops were obtained at lower temperatures. The polarization value could be determined from the current hysteresis by integrating the switching peak on the positive polarity, after extracting the leakage current contribution (see eq SE1 in the Supporting Information). The values are about the same, in the 21−25 $\mu C/cm^2$ range. As regarding the imprint, it was found that at least for top Pt and SRO electrodes it has the same orientation as in the case of PZT, suggesting similar origin.

The hysteresis loop for the case of the top Al contact requires significantly higher voltages to reverse the polarization, suggesting the presence of a layer of oxidized aluminum (possible Al_2O_3) at the interface. The higher voltages imply also a larger contribution from the part of the leakage current (see Figure S4 in the Supporting Information). However, the estimated polarization is in the same range as for the other metals used for top contacts.

The influence of the top electrode interface is also evident in the case of the $C-V$ characteristics. The dielectric constants calculated from the capacitance values measured at voltage where the polarization is saturated (see Figure 1d) are different for different materials used as top contacts, implying that the

related dielectric constant is not a property of the ferroelectric layer but of the overall MFM structure. Regarding the values, one can see that: in the case of the PZT the spread is lower than in the case of the BTO; the average value for the PZT is about 143, whereas that for BTO is about 300; for Al, the value of the obtained dielectric constant is lower, suggesting again the presence of a thin oxidized aluminum layer with low capacity at the interface (see also Figure S7 in the Supporting Information).

The $I-V$ measurements at different temperatures were used to estimate the height of the potential barrier at the two electrode interfaces by assuming that the charge transport through the MFM structure is governed by the Schottky-Simmons equation, and that the MFM structure can be assimilated with a back-to-back connection of two Schottky diodes associated to the electrode interfaces (see Equation SE2 in the Supporting Information).[34] Similar procedures were used to analyze the leakage current mechanisms in other ferroelectric materials.[35,36] This means on one hand that the charge injection is controlled by the interface through the potential barrier and the drift-diffusion is controlled by the bulk through the charge carrier mobility, and on the other hand that no matter the polarity of the applied voltage one of the electrode interfaces will be reverse biased and will limit the current. An example for the application of the Schottky−Simmons formalism to extract the height of the potential barrier is shown in Figure 2a−c for the symmetric MFM structure SRO-PZT-SRO (more details in Supporting Information paragraph $I-V$ characteristics). First, the $\ln(J/T^{3/2}) \sim 1000/T$ dependence is represented for several voltages, and the apparent potential barrier is extracted from the slope. Then, the apparent potential barriers are represented as function of $V^{1/2}$. The dependence must be linear and from the intercept at origin the height of the potential barrier at zero volts is extracted. The results obtained for the materials used as top contacts are presented in the Table 1.

The striking result is that, except top Al contacts, the values obtained for the potential barriers at room temperature are about the same, within 0.1 and 0.3 eV, both for PZT and BTO, no matter the material used for top contact. The result is puzzling considering that the work function difference between Pt and Cu is of 1 eV. Only in the case of top Al the potential barriers are higher, of about 0.4 eV in the case of PZT and about 0.8−0.9 eV in the case of BTO layer. This result also support the presence of a thin layer of aluminum oxide at the top electrode interface, with insulating properties (similar to metal-insulating-semiconductor MIS diodes[37]).

Another striking result is the fact that the height of the potential barrier does not depend on the polarity of the applied voltage. We remind here that all the top contacts are deposited on the same ferroelectric film, with the same SRO bottom electrode. Assuming a back-to-back connection of two Schottky diodes, one would expect that for one polarity the height of the potential barrier remains the same, being associated to the bottom SRO−ferroelectric interface, which does not change, whereas for the opposite polarity, the height will change, being associated with the top electrode−ferroelectric interface. This is not the case, as long as for top Al on BTO the height of the potential barrier is significantly increasing for both polarities. The increased barrier at the top interface can be explained by the presence of the thin oxidized aluminum layer. However, the increased barrier at the bottom interface can be explained only accepting that the ferroelectric polarization is inducing

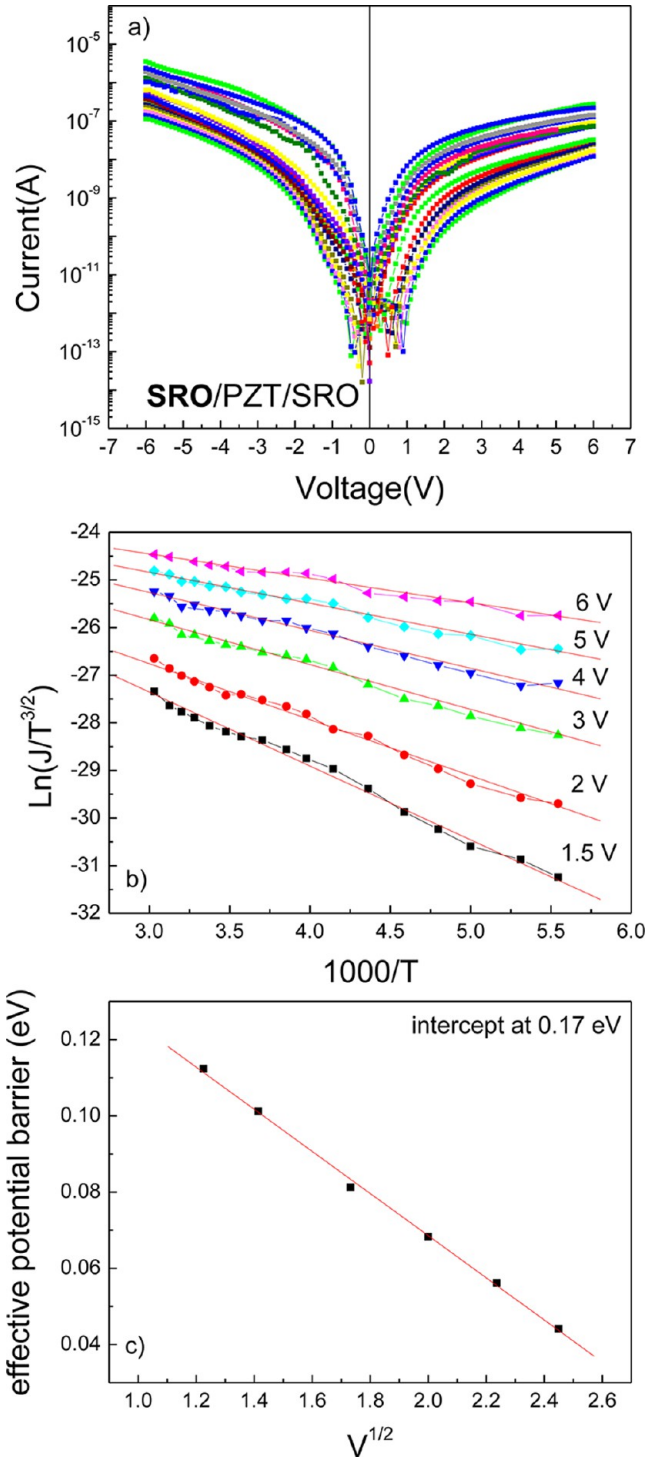

Figure 2. Example of the procedure used to extract the height of the potential barrier from the $I-V$ measurements applied for a SRO-PZT-SRO capacitor: (a) the $I-V$ characteristics at different temperatures; (b) the $\ln(J/T^{3/2}) \sim 1000/T$ representation derived from the Schottky−Simmons equation (positive polarity); (c) the $V^{1/2}$ dependence of the effective potential barrier used to extract the potential barrier at zero volts.

"symmetry" in the structure, reflected also in the macroscopic electrical properties (see the $C-V$ characteristic and hysteresis loop for top Al on BTO in the Supporting Information).

3.2. Microscopic Analysis. *3.2.1. XPS Investigations.* To gain more insight regarding the formation of the electrode−

Table 1. Height of Potential Barriers (in eV, at room temperature) for the SRO, Pt, Cu, Al, and Au Top Contacts, and for the Two Polarities of the Applied Voltage on the Top Electrode, along with work functions (in eV)

	PZT					BTO				
	SRO	Pt	Cu	Al	Au	SRO	Pt	Cu	Al	Au
Φ_B^0 (eV) positive polarity	0.14	~0.1	0.11	0.38	0.26	0.21	0.22	0.19	0.92	0.31
Φ_B^0 (eV) negative polarity	0.17	0.16	0.11		0.3	0.22	0.19	0.23	0.79	
work function	4.7−4.9	5.65	4.65	4.28	5.1	4.7−4.9	5.65	4.65	4.28	5.1

ferroelectric interface X-ray photoelectron spectroscopy (XPS) was used, by following a methodology recently published.[38−40] Cu, Au, and Pt layers were deposited by molecular beam epitaxy on the surface of the ferroelectric film, which was previously heated in the analysis chamber at 400 °C in ultrahigh vacuum (UHV, 1×10^{-9} to 1×10^{-10} mbar), in order to remove the surface contaminants, especially carbon (see details in the Supporting Information). It was found that, after the annealing in UHV, the C content on the surface is less than one-quarter of an atomic layer. This was considered good enough for metal deposition. Also, a slight progressive n doping is visible through the increase in the $E_F - E_V$ difference with heating[39] in the valence band region. However, the overall surface composition is not much affected by this annealing process.[40] The deposition was sequential, starting with 2 Å and ending with a thickness of 10 nm. After each metal deposition, the XPS spectra were recorded. It was possible in this way to monitor the shift of the binding energies for the core level electrons of Pb 4f, Ti 2p, Zr 3d, and O 1s in the case of PZT, and Ba 3d, Ba 4d, Ti 2p, and O 1s in the case of BTO. For 10 nm thickness of the metal electrode, the signals from the ferroelectric material's atoms were strongly attenuated for Cu and Pt deposition, but were still visible for Au deposition. This suggests that the ferroelectric layer was completely covered by Cu and Pt, but uncompletely covered by Au.[38] Figure 3 presents shifts of the main components originating from the ferroelectric film for all samples investigated, together with the dependence of the levels provided by the metal film (Au 4f, Cu 2p, and Pt 4f). The corresponding XPS spectra, together with their simulation with several components are presented in the Supporting Information.

The XPS investigation of the low binding energy region (valence band) has revealed that the position of the Fermi level is close to midgap (see details in the Supporting Information). One has to mention that the position of the Fermi level before and after the metal deposition does not differ. This is because all the time the sample was kept at the same potential with the rest of the experimental setup. The difference between the Fermi level and the maximum of the valence band is of about 1.6−1.9 eV for PZT and BTO, both having a band gap of about 3.5−3.9 eV.[41−43] The results are consistent with the values of 1.6−1.8 eV reported for Cu, Pt and Ag deposited on PZT.[18] and with the values reported for Au[38] films deposited on PZT without thermal treatment, i.e. when a contamination layer is present on the ferroelectric layer before metal deposition. This result can be explained assuming that either the investigated ferroelectrics are almost intrinsic, or that the Fermi level is pinned near midgap by some deep trapping level. We affirm here that the Fermi level should be near mid gap in a MFM structure based on epitaxial ferroelectric films because the bulk of the film is totally depleted of free charges (intrinsic behavior), and these free charges accumulates in a thin region near electrode interfaces to compensate the bound polarization charges. Using the $C-V$ characteristics in the same way as for a metal-ferroelectric Schottky diode we can make an estimate of the free carrier concentrations in PZT and BTO layers, using the dielectric constants determined from the capacitance measurements. The results are in the range $(8-10) \times 10^{23}$ m^{-3} for BTO and $(4-10) \times 10^{24}$ m^{-3} for PZT (see eq SE3 and Figure S12 in the Supporting Information). The above free charge concentrations can be converted in surface charge densities, knowing that the film thickness is 300 nm. It results that this charge can compensate maximum 5 $\mu C/cm^2$ in BTO and 40 $\mu C/cm^2$ in PZT films. The amount of polarization charges that can be compensated by the free charges that are present in the ferroelectric films is well below the polarization estimated from the hysteresis measurements in the case of the BTO or PZT films. It results that no free charges are present in the bulk of the film, in agreement with the close to mid gap position of the Fermi level. The fact that the Fermi level is not exactly mid gap can be due to the fact that structural defects are still present in the film (vacancies, dislocations) although the structure is of good epitaxial quality. These defects introduce energy levels in the forbidden band, slightly affecting the position of the Fermi level.

Regarding Figure 3, one can be surprised that the shifts are similar for both PZT and BTO layers, namely to higher values in the case of Au (~0.2 eV for PZT; ~0.4 eV for BTO), suggesting a downward band-bending at the Au−-ferroelectric interface, and to lower values in the case of Cu (~0.3 eV for PZT; ~0.06 eV for BTO), suggesting an upward band-bending at the Cu−ferroelectric interface. Considering these results one can say that Au forms nonrectifying ohmic-like contacts for electrons,[44] whereas Cu forms rectifying-like contacts. The results are not entirely in agreement with those obtained from macroscopic $I-V$ measurements because a potential barrier was determined for Au also. The results obtained for Pt are similar to those obtained in the case of Au (higher binding energies, with about 0.7−0.8 eV, see the Supporting Information).

One can observe that the binding energies of the core levels before depositing the metal layer are not exactly the same for all samples (see Figure 3). For example, the binding energy for Ti 2p main component is 459.0, 458.2, and 457.7 eV for Cu, Au, and Pt, respectively. In ref 16. it is mentioned that the binding energies are dependent on the polarization orientations, with values of 458.8 eV for P^+ (outward polarization) and 457.6 eV for P^- (inward polarization). The value for P^0 (zero macroscopic polarization) is in between. The P^0 state can be obtained either by forming domains with opposite orientations of out-of-plane polarization or by having in-plane polarization. The values in Figure 3 are in exactly the same range as in ref 16. This fact suggests that the three samples are not in the same polarization state. It appears that the Cu was deposited on a sample having mostly P^+ orientation, Au was deposited on a sample having mostly P^0 orientation, whereas Pt was deposited on a sample having mostly P^- orientation. The different polarization states may be due to various reasons: the different amount of the structural defects (especially vacancies); the

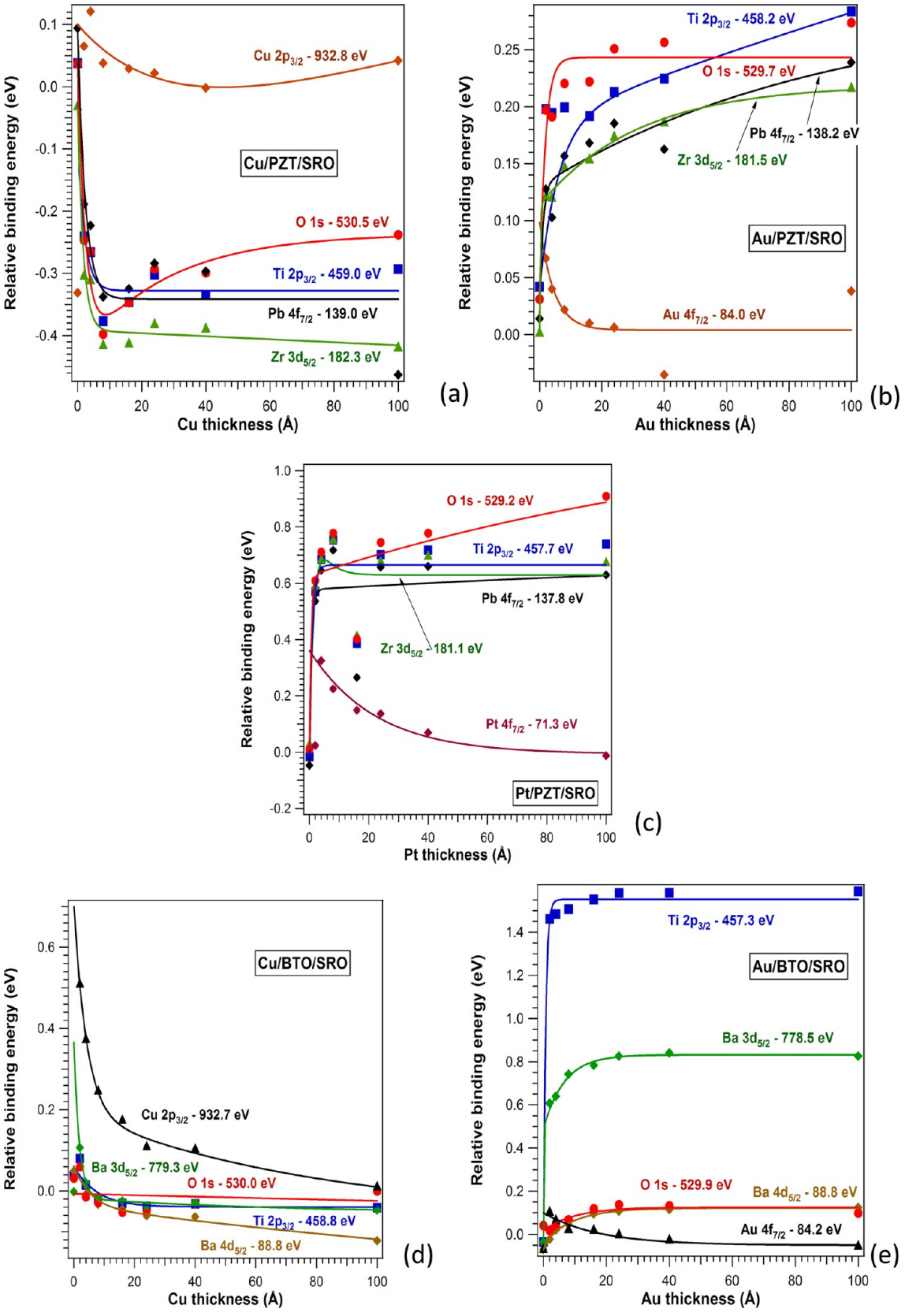

Figure 3. Core level shifts of the major components obtained by simulation for (a) Cu/PZT/SRO, (b) Au/PZT/SRO, (c) Pt/PZT/SRO, (d) Cu/BTO/SRO, and (e) Au/BTO/SRO.

quality of the STO substrate, with impact on the strain in the deposited layers; the time elapsed from the sample preparation to their introduction in UHV.[40] As long as no electric field is applied to setup a certain direction of polarization, the polarization state can be different even the history of the samples is about the same. Furthermore, the polarization state

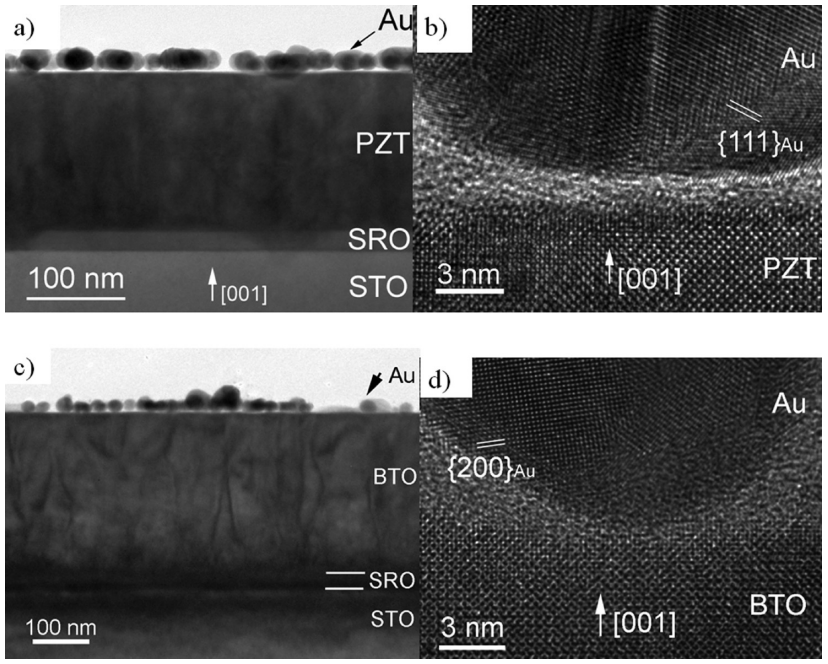

Figure 4. (a) Low-magnification TEM image of the Au/PZT/SRO/STO sampl; (b) HRTEM image at the Au-PZT interface; (c) low-magnification TEM image of the Au/BTO/SRO/STO sample; (d) HRTEM image at the Au-BTO interface.

may change during the metal deposition by MBE.[45] In any case, the binding energies after metal deposition are the same within the experimental errors (~0.1 eV): 458.7 eV for Cu; 458.5 eV for Au, and 458.5 for Pt. This fact suggests that the polarization state of the three samples after metal deposition is almost the same. This can be explained by the fact that the top metal layer is short-circuiting the ferroelectric layer thus the compensation charges cancel each other at the two interfaces.[45] The result is a state with dominant P^0 orientation, with only small areas having out-of-plane polarization.

Finally, the Schottky barrier for electrons was estimated from the XPS measurements. The obtained values are, in the case of the PZT layer, 1.4 eV for Cu, 1.6 eV for Au, and 1.65 eV for Pt; in the case of the BTO layer, 1.6 eV for Cu and 1.5 eV for Au. These values are not very different, considering the work function difference of about 1 eV between Cu and Pt, and are in good agreement with previous reports.[18] However, they are much larger than the values obtained from the $I-V$ measurements. This aspect will be commented in the Discussion section.

3.2.2. HR-TEM Investigations. Complementary to XPS investigations the HR-TEM was used to further analyze the interface between the Cu, Au, Pt electrodes and the ferroelectric layer, on the same samples prepared in MBE chamber and used for XPS. One has to mention from the beginning that, during the TEM sample preparation, it was observed that the metal layers deposited by MBE method on the PZT surface are not adherent. Special care was needed to obtain good samples for TEM investigation although excess C contamination compared to XPS results could not be avoided during the sample preparation (see also the Supporting Information, Figure S19, and the related text for Cu on PZT).

The TEM analysis reveals the fact that Au deposited by MBE is forming nanoparticles on the surface of the ferroelectric layer (see Figure 4). Therefore, the 10 nm thick Au layer is not continuous, in line with the persistence of Au signal observed by XPS after 10 nm Au deposition, and a thin parasitic layer seems to form at the interface with the ferroelectric. This can be due to the poor adherence of the MBE deposited Au on the surface of the PZT layer. The small dielectric gap can induce a potential barrier[46,47] although the higher binding energies detected by XPS suggest downward band bending corresponding to nonrectifying contacts. On the other hand, Cu seems to form a continuous layer. The chemical analysis performed in the scanning TEM mode has revealed the presence of an oxidized Cu layer at the interface, as shown in Figure 5 for the case of PZT (more details in the Supporting Information). That would explain the rectifying behavior of the Cu-ferroelectric interface. The results of the TEM analysis for Pt are similar to those obtained in the case of Au.

3.3. Discussion. The experimental results of the macroscopic electrical measurements and of the microscopic investigations performed by XPS and HR-TEM convey toward the same conclusion: the overall behavior of the electrode-ferroelectric interface is about the same no matter the ferroelectric material. Furthermore, the electronic properties of the electrode interface seem to be almost independent of the materials used for electrodes and on the voltage polarity. We remind here the bottom electrode was in all cases SRO. Materials with very different properties were used as top contacts. Nevertheless, the overall behavior of the ferroelectric capacitor remains fairly symmetric although the top and bottom electrodes are very asymmetric.

The results can be explained only accepting that the bound charge associated to ferroelectric polarization is setting up the band-bending and the height of the potential barrier at the electrode-ferroelectric interface. The work function is not important in this case, only the magnitude of ferroelectric polarization is important and the quality of the interface.

The discrepancy between the values of the potential barriers estimated from the XPS measurements and those estimated from the $I-V$ characteristics may be only apparent. First, one have to mention that the $I-V$ measurement is a dynamic one, having all the time an electric field applied on the sample in

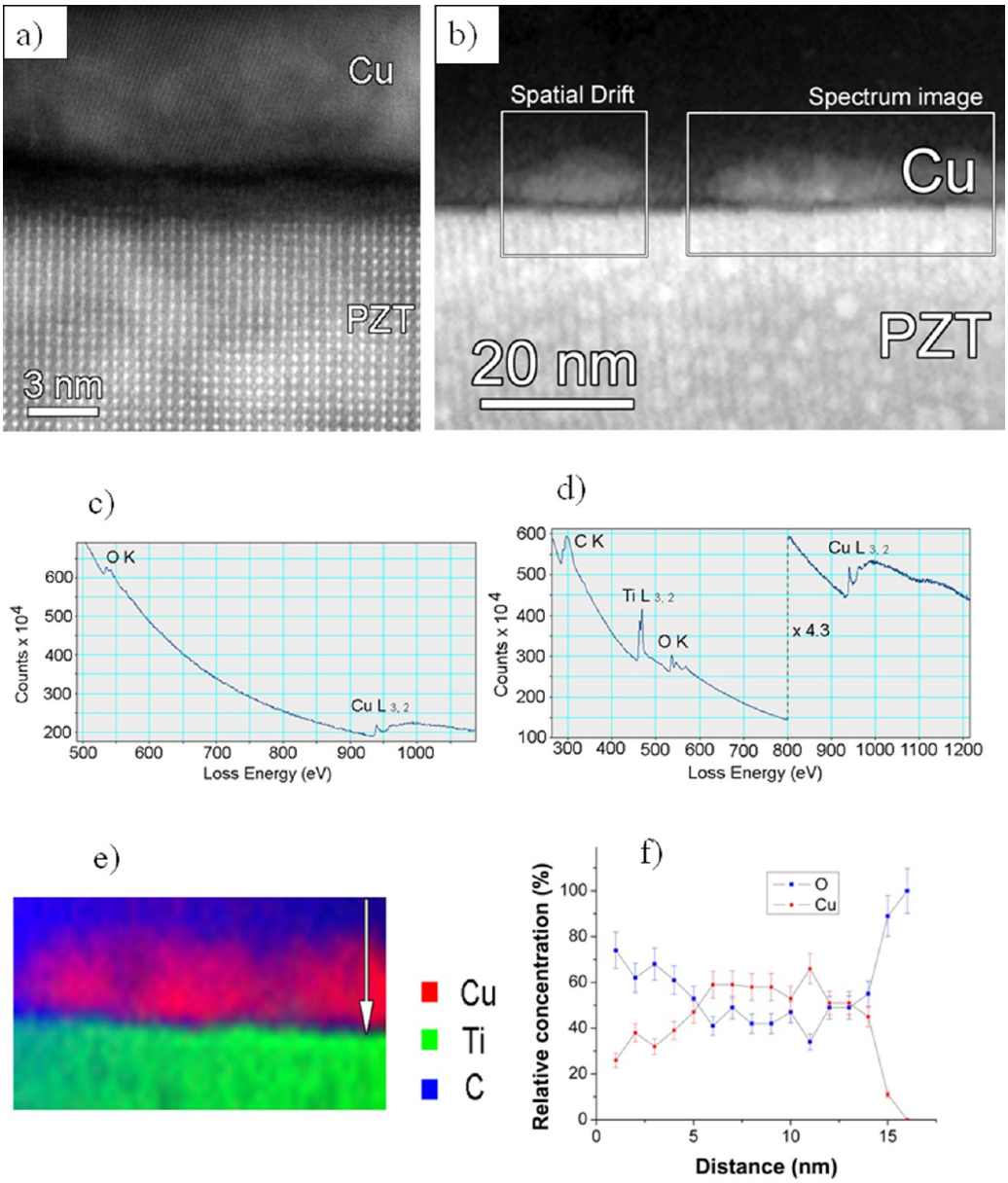

Figure 5. (a) High-resolution HAADF-STEM image of the interface between the epitaxial PZT layer and the Cu layer used as outer electrode; (b) low-magnification HAADF-STEM image used for acquisition of the spectrum image around the Cu-PZT interface (denoted area); (c) EEL spectrum extracted from the whole area of the spectrum image showing the Cu $L_{3,2}$, O K, Ti $L_{3,2}$, and C K edges; (d) EEL spectrum extracted from a narrow area inside the Cu layer; (e) composite RGB image showing the spatial distribution of Cu, Ti, and C inside the area denoted "spectrum image"; (f) plot of the Cu and O content along the arrow crossing the Cu layer on the composite RGB elemental map.

order to maintain a certain out-of-plain direction of polarization. The *I*−*V* curves are obtained when voltages are decreased in absolute values, once sufficient voltage is applied in order to polarize the ferroelectric layer. Therefore, electrons are injected into the layer by the electrode set at negative voltage, and this yields a displacement of the Fermi level toward the conduction band. Each *I*−*V* branch is measured once the sample is "saturated" with electrons. On the other hand, XPS is a static measurement, with no electric field applied on the sample, and leading at the end (after metal deposition) to a dominant P^0 polarization state (almost no out-of-plane macroscopic polarization present).[45] Second, the XPS estimations assume that the standard band calculations used for metal-semiconductor contacts are valid also in the case of ferroelectrics, neglecting the influence of the polarization bound charges although it is accepted that these can affect the band-bending at the surface/interface.[14,15] However, the position of the Fermi level extracted from XPS investigations is supporting the idea that the electronic properties of the ferroelectric capacitor, including the electrode interfaces, are controlled by the polarization charges. Assuming an ideal ferroelectric layer, with a polarization oriented perpendicular to the electrode interfaces then it is clear that all the free charges existing in the film will go toward the interfaces to compensate the depolarization field (see Figure 6a).

The bound polarization charges located just near the interfaces are requiring compensation charges of opposite sign.[48] The compensation charges are coming from the ferroelectric film or from the electrodes, forming a cloud just near the interface.[46,47] The overall charge density in the MFM

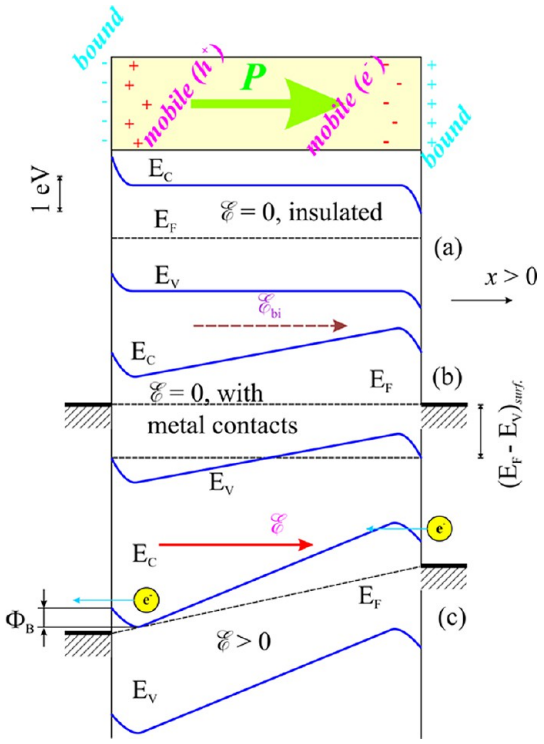

Figure 6. Schematic of the MFM structure. The upper panel presents a sketch of the film, with bound (blue) and compensation (red) charges for a given orientation of the spontaneous polarization *P*, in the ideal case when the total electric field and the total electric charges in the structure should be zero. (a) Band diagram for the given orientation of polarization and without applied electric field, in the ideal case when the sample is insulated and not connected to ground on both sides; (b) band diagram without an applied voltage, but for both sides of the film held at the same potential (grounded); (c) the case with an applied electric field ϵ. Notations are as follows: E_C, conduction band edge; E_F, Fermi level; E_v, valence band edge; e, electron; Φ_B, the "apparent" Schottky barrier determined from the experimental *I*−*V* measurements.

structure will be zero. This is the situation of an intrinsic wide gap semiconductor with negligible density of intrinsic carriers at room temperature. At the interface where the bound charges are negative the energy bands will be bend upward as for depletion of electrons and accumulation of holes.[38] At the other interface the energy bands will be bend downward, as for electron accumulation and holes depletion (see Figure 6a). Similar band bending is present if contacts are added to the ferroelectric layer, with the mention that a nonzero internal electric field is present although no external field is applied on the MFM structure.[49] When an electric field is applied on the MFM structure, preserving the polarization orientation (see Figure 6c), then electrons will be pushed from the right contact, through the ferroelectric film, toward the left interface with negative bound charges. The right contact acts as an ohmic contact[44] injecting electrons into the film. The electron accumulation at the left contact can alter the positive compensation charges, destabilizing the polarization. To prevent this, the electrons had to overcome the upward band bending noted as Φ_B. This is in fact the "apparent potential barrier" determined from the *I*−*V* measurements. One can say that the polarization is "adjusting" the height of this barrier in such a way that its orientation is not affected. The upward shift of the Fermi level throughout the structure (see Figure 6c) is only suggesting the n-type doping induced by the external electric field injecting electrons at the right contact.

If the applied electric field is in opposite direction to the polarization then the compensation charges will be pulled from the interfaces into the external circuit. This situation is favored by the band bending shown in Figure 6b. The polarization becomes unstable and, at the coercive field, it will switch. The switch will be accompanied by a change in band bending, upward becoming downward and vice versa. The change in band bending will block the flow of charge into the ferroelectric film stabilizing the new orientation of polarization parallel to the applied electric field. One has to note that the compensation charges are already available in the circuit when the switching take place, explaining the rapid switching and the rectangular shape of the hysteresis loop. Any defect altering the flow of charge during switching will delay the compensation, leading to back-switching effects due to the incomplete annihilation of the depolarization field.[46,47] Therefore, one can conclude that slightly rectifying contacts, with properties controlled by the bound polarization charges are required to stabilize the polarization orientation and to obtain rectangular hysteresis loops. If both contacts would be ohmic, then no orientation of polarization would be stable because the free charges will flow freely through the circuit, making impossible the compensation of the depolarization field. This is a strong experimental support for the Vanderbilt's surface/interface theorem.[29] Referring to Figure 6, this is only qualitative representation trying to reconcile the results of the *I*−*V* measurements and XPS investigation. Detailed theoretical models have to be developed in order to accurately simulate the band-bending in correlation with the experimental *I*−*V* and XPS results. An eventual decrease in the band bending associated with the ferroelectric polarization due to excess charge carriers near metal interfaces might also be taken into account, although the estimated carrier densities from C−V characteristics are 2−3 orders of magnitude lower than the charge density, which was computed by Landau−Ginsburg−Devonshire theory to yield significant decrease of the permanent ferroelectric polarization.[48] Nevertheless, eventual significant charge accumulation at metal interfaces will result in a further reduction of the band bending represented in Figure 6b.

Some attempts to study the effect of the different metals as electrodes on ferroelectric layers with polycrystalline structure were made.[50−52] However, in terms of the leakage current, it seems that the conduction mechanisms can be significantly different from those reported for ferroelectric layers of epitaxial quality. This is understandable if one consider that, because of its the polycrystalline nature, the bulk of the film may take the control over the macroscopic electrical properties, making the effect of the electrode interfaces almost negligible.[53,54]

3. CONCLUSIONS

The fact that the same behavior is obtained on two different ferroelectric materials, using the same metals as electrodes support the conclusion that the polarization control of the electronic properties of the electrode interfaces is a general phenomena. It may depend, however, on the thickness of the ferroelectric film. If the film is too thin then the two interfaces may interact, leading to totally different electrical properties at macroscopic level such as collapse of the dielectric constant, increased leakage current due to tunneling effects, etc.[55,56]

We think that the above results bring completely new knowledge about the formation of the electrode interfaces on surfaces carrying sheets of bound charges like in the case of ferroelectrics. The results can be of interest not only for the peoples who work in the field of ferroelectric materials and related applications but also for peoples working on polar materials in general (e.g., polar semiconductors like ZnO, GaN, or electrets).[57,58] Knowing how to control the properties of the electrode interfaces can be a valuable tool in the development of the new devices for nonvolatile memories based on field effect, tunneling junctions (combination of tunneling magneto-resistance and electro-resistance), or on resistive switching, and involving either inorganic or organic/polymer materials with ferroelectric properties.[59−64]

■ ASSOCIATED CONTENT

Supporting Information

Details regarding the structural characterization of the films, the procedures and methods used to extract relevant quantities from the electrical measurements (e.g., polarization value in the case of a hysteresis loop affected by the leakage current, the density of the free carriers, the height of the potential barrier at the electrode−ferroelectric interface), the XPS investigation (examples of spectra analysis, C contamination, example of spectra used to extract the position of the valence band maximum with respect of the Fermi level), and the TEM investigation (including oxygen content). This material is available free of charge via the Internet at http://pubs.acs.org/.

■ AUTHOR INFORMATION

Corresponding Author

*E-mail: pintilie@infim.ro. Phone +40.21.369.0170. Fax: +40.21.369.0177

Notes

The authors declare no competing financial interest.

■ ACKNOWLEDGMENTS

The authors acknowledge the financial support of the Romanian Ministry of Education-Executive Unit for Funding High Education, Research, Development and Innovation (MEN-UEFISCDI) through the Idea-Complex Research Grant PN-II-ID-PCCE-2011-2-0006 (Contract 3/2012).

■ REFERENCES

(1) Uchino, K., *Ferroelectric Devices*; Marcel Dekker: New York, 2000.
(2) Scott, J. F., *Ferroelectric Memories*; Itoh, K., Sakurai, T., Eds.; Advanced Microelectronics Series; Springer-Verlag: Berlin, 2000; Vol. 3.
(3) Duan, C. G.; Sabirianov, R. F.; Mei, W. N.; Jaswal, S. S.; Tsymbal, E. Y. Interface Effect on Ferroelectricity at the Nanoscale. *Nano Lett.* **2006**, *6*, 483−487.
(4) Stengel, M.; Vanderbilt, D.; Spaldin, N. A. Enhancement of Ferroelectricity at Metal−Oxide Interfaces. *Nat. Mat.* **2009**, *8*, 392−397.
(5) Stengel, M.; Puente, A. P.; Spaldin, N. A.; Junquera, J. Band Alignment at Metal/Ferroelectric Interfaces: Insights and Artifacts from First Principles. *Phys. Rev. B* **2011**, *83*, 235112.
(6) Chu, M. W.; Szafraniak, I.; Scholz, R.; Harnagea, C.; Hesse, D.; Alexe, M.; Gösele, U. Impact of Misfit Dislocations on the Polarization Instability of Epitaxial Nanostructured Ferroelectric Perovskites. *Nat. Mater.* **2004**, *3*, 87−90.
(7) Zubko, P.; Gariglio, G.; Gabay, M.; Ghosez, P.; Triscone, J. M. Interface Physics in Complex Oxide Heterostructures. *Annu. Rev. Condens. Matter Phys.* **2011**, *2*, 141−165.
(8) Stengel, M.; Spaldin, N. A. Origin of the Dielectric Dead Layer in Nanoscale Capacitors. *Nature* **2006**, *443*, 679682.
(9) Chang, L. W.; Alexe, M.; Scott, J. F.; Gregg, J. M. Settling the "Dead Layer" Debate in Nanoscale Capacitors. *Adv. Mater.* **2009**, *21*, 4911−4914.
(10) Stephanovich, V. A.; Glinchuk, M. D.; Zaulychny, V. Y. Exact and Variational Treatment of Ferroelectric Thin Films with Different Materials of Electrodes. *Ferroelectrics* **2005**, *317*, 293−299.
(11) Yang, Y. S.; Lee, S. J.; Yi, S.; Chae, B. G.; Lee, S. H.; Joo, H. J.; Jang, M. S. Schottky Barrier Effects in the Photocurrent of Sol−gel Derived Lead Zirconate Titanate Thin Film Capacitors. *Appl. Phys. Lett.* **2000**, *76*, 774−776.
(12) Lee, D.; Baek, S. H.; Kim, T. H.; Yoon, J.-G.; Folkman, C. M.; Eom, C. B.; Noh, T. W. Polarity Control of Carrier Injection at Ferroelectric/Metal Interfaces for Electrically Switchable Diode and Photovoltaic Effects. *Phys. Rev. B* **2011**, *84*, 125305.
(13) Weida, W.; Guest, J. R.; Horibe, Y.; Park, S.; Choi, T.; Cheong, S.-W.; Bode, M. Polarization-Modulated Rectification at Ferroelectric Surfaces. *Phys. Rev. Lett.* **2010**, *104*, 217601.
(14) Huang, B. C.; Chen, Y. T.; Chiu, Y. P.; Huang, Y. C.; Yang, J. C.; Chen, Y. C.; Chu, Y. H. Direct Observation of Ferroelectric Polarization-Modulated Band Bending at Oxide Interfaces. *Appl. Phys. Lett.* **2012**, *100*, 122903.
(15) Rault, J. E.; Agnus, G.; Maroutian, T.; Pillard, V.; Lecoeur, Ph.; Niu, G.; Vilquin, B.; Silly, M. G.; Bendounan, A.; Sirotti, F.; Barrett, N. Interface Electronic Structure in a Metal/Ferroelectric Heterostructure under Applied Bias. *Phys. Rev. B* **2013**, *87*, 155146.
(16) Chen, F.; Klein, A. Polarization Dependence of Schottky Barrier Heights at Interfaces of Ferroelectrics Determined by Photoelectron Spectroscopy. *Phys. Rev. B* **2012**, *86*, 094105.
(17) Chen, F.; Schafranek, R.; Wu, W.; Klein, A. Formation and Modification of Schottky Barriers at the PZT/Pt Interface. *J. Phys. D: Appl. Phys.* **2009**, *42*, 215302.
(18) Chen, F.; Schafranek, R.; Wu, W.; Klein, A. Reduction-Induced Fermi Level Pinning at the Interfaces between $Pb(Zr,Ti)O_3$ and Pt, Cu, and Ag Metal Electrodes. *J. Phys. D: Appl. Phys.* **2011**, *44*, 255301.
(19) Juan, P. C.; Chou, H. C.; Lee, J. Y. M. The Effect of Electrode Material on the Electrical Conduction of Metal-$Pb(Zr_{0.53}Ti_{0.47})O_3$-Metal Thin Film Capacitors. *Microelectron. Reliab.* **2005**, *45*, 1003−1006.
(20) Stolichnov, I.; Tagantsev, A.; Setter, N.; Cross, J. S.; Tsukada, M. Control of leakage conduction of high-fatigue-endurance (Pb,La)-$(Zr,Ti)O_3$ film ferroelectric capacitors with Pt/SrRuO3 electrodes. *Appl. Phys. Lett.* **1999**, *75*, 1790−1792.
(21) Pintilie, L.; Vrejoiu, I.; Hesse, D.; Le Rhun, G.; Alexe, M. Ferroelectric Polarization-Leakage Current Relation in High-Quality Epitaxial $Pb(Zr,Ti)O_3$ Films. *Phys. Rev. B* **2007**, *75*, 104103.
(22) Picinin, A.; Lente, M. H.; Eiras, J. A.; Rino, J. P. Theoretical and Experimental Investigations of Polarization Switching in Ferroelectric Materials. *Phys. Rev. B* **2004**, *69*, 064117.
(23) Pintilie, L. Advanced Electrical Characterization of Ferroelectric Thin Films: Facts and Artifacts. *J. Optoelectron. Adv. Mater.* **2009**, *11*, 215−228.
(24) Araujo, E. B.; Eiras, J. A. Effects of Crystallization Conditions on Dielectric and Ferroelectric Properties of PZT Thin Films. *J. Phys. D: Appl. Phys.* **2003**, *36*, 2010−2013.
(25) Vrejoiu, I.; Le Rhun, G.; Pintilie, L.; Hesse, D.; Alexe, M.; Gösele, U. Intrinsic Ferroelectric Properties of Strained Tetragonal, $PbZr_{0.2}Ti_{0.8}O_3$ Obtained on Layer-by-Layer Grown, Defect-Free Single-Crystalline Films. *Adv. Mater.* **2006**, *18*, 1657−1661.
(26) Kim, T. H.; Baek, S. H.; Yang, S. M.; Kim, Y. S.; Jeon, B. C.; Lee, D.; Chung, J.-S.; Eom, C. B.; Yoon, J.-G.; Noh, T. W. Polarity-Dependent Kinetics of Ferroelectric Switching in Epitaxial $BiFeO_3(111)$ Capacitors. *Appl. Phys. Lett.* **2011**, *99*, 012905.
(27) Choi, T.; Lee, S.; Choi, Y. J.; Kiryukhin, V.; Cheong, S.-W. Switchable Ferroelectric Diode and Photovoltaic Effect in $BiFeO_3$. *Science* **2009**, *324*, 63−66.
(28) Pintilie, L.; Dragoi, C.; Chu, Y. H.; Martin, L. W.; Ramesh, R.; Alexe, M. Orientation-Dependent Potential Barriers in Case of

Epitaxial Pt−$BiFeO_3$−$SrRuO_3$ Capacitors. *Appl. Phys. Lett.* **2009**, *94*, 232902.
(29) Vanderbilt, D.; King-Smith, R. D. Electric Polarization As a Bulk Quantity and Its Relation to Surface-Charge. *Phys Rev. B* **1993**, *48*, 4442−4455.
(30) Stengel, M.; Vanderbilt, D.; Spaldin, N. A. First-Principles Modeling of Ferroelectric Capacitors via Constrained Displacement Field Calculations. *Phys. Rev. B* **2009**, *80*, 224110.
(31) Hrib, L. M.; Boni, A. G.; Chirila, C.; Pasuk, I.; Pintilie, I.; Pintilie, L. Electrode Interface Control of the Schottky Diode-like Behavior in Epitaxial $Pb(Zr_{0.2}Ti_{0.8})O_3$ Thin Films: A Critical Analysis. *J. Appl. Phys.* **2013**, *113*, 214108.
(32) *CRC Handbook of Chemistry and Physics*, 76th ed.; Lide, D. R., Ed.; CRC Press: Boca Raton, FL, 1995.
(33) Hartmann, A. J.; Neilson, M.; Lamb, R. N.; Watanabe, K.; Scott, J. F. Ruthenium Oxide and Strontium Ruthenate Electrodes for Ferroelectric Thin-Films Capacitors. *Appl. Phys. A: Mater. Sci. Process.* **2000**, *70*, 239−242.
(34) Chai, F. K.; Brews, J. R.; Schrimpf, R. D.; Birnie, D. P. Limitations of the Uniform Effective Field Approximation Due to Doping of Ferroelectric Thinfilm Capacitors. *J. Appl. Phys.* **1995**, *78*, 4766−4775.
(35) Wu, J.; Wang, J.; Xiao, D.; Zhu, J. Migration Kinetics of Oxygen Vacancies in Mn-Modified $BiFeO_3$ Thin Films. *ACS Appl. Mater. Interfaces* **2011**, *3*, 2504−2511.
(36) Wu, J.; Wang, J.; Xiao, D.; Zhu, J. Leakage Mechanism of Cation-Modified $BiFeO_3$ Thin Film. *AIP Adavances* **2011**, *1*, 022138.
(37) Moret, M. P.; Devillers, M. A. C.; Worhoff, K.; Larsen, P. K. Optical Properties of $PbTiO_3$, $PbZr_xTi_{1-x}O_3$, and $PbZrO_3$ Films Deposited by Metalorganic Chemical Vapor on $SrTiO_3$. *J. Appl. Phys.* **2002**, *92*, 468−474.
(38) Apostol, N. G.; Stoflea, L. E.; Lungu, G. A.; Chirila, C.; Trupina, L.; Negrea, R. F.; Ghica, C.; Pintilie, L.; Teodorescu, C. M. Charge Transfer and Band Bending at Au/$Pb(Zr_{0.2}Ti_{0.8})O_3$ Interfaces Investigated by Photoelectron Spectroscopy. *Appl. Surf. Sci.* **2013**, *273*, 415−425.
(39) Apostol, N. G.; Stoflea, L. E.; Lungu, G. A.; Tanase, L. C.; Chirila, C.; Frunza, L.; Pintilie, L.; Teodorescu, C. M. Band Bending in Au/$Pb(Zr,Ti)O_3$ Investigated by X-ray Photoelectron Spectroscopy: Dependence on the Initial State of the Film. *Thin Solid Films* **2013**, *545*, 13−21.
(40) Apostol, N. G.; Stoflea, L. E.; Lungu, G. A.; Tache, C. A.; Pintilie, L.; Teodorescu, C. M. Band Bending at Free $Pb(Zr,Ti)O_3$ Surfaces Analyzed by X-ray Photoelectronspectroscopy. *Mater. Sci. Eng., B* **2013**, *178*, 1317−1322.
(41) Lee, H.; Kang, Y. S.; Cho, S.-J.; Xiao, B.; Morkoç, H.; Kang, T. D.; Lee, G. L.; Li, J.; Wei, S.-H.; Snyder, P. G.; Evans, J. T. Dielectric Functions and Electronic Band Structure of Lead Zirconate Titanate Thin Films. *J. Appl. Phys.* **2005**, *98*, 094108.
(42) Peacock, P. W.; Robertson, J. Band Offsets and Schottky Barrier Heights of High Dielectric Constant Oxides. *J. Appl. Phys.* **2002**, *92*, 4712−4721.
(43) Lee, W.-S.; Ahn, K.-C.; Yoon, S.-G.; Kim, C. S. Effect of Film Thickness on the Ferroelectric Properties of $Pb(Zr_{0.2}Ti_{0.8})O_3$ Thin Films for Nano-data Storage Applications. *J. Vac. Sci. Technol. B* **2005**, *23*, 1901−1904.
(44) Kao, K. C. *Dielectric Phenomena in Solids*; Elsevier Academic Press: Waltham, MA, 2004; Chapter 6, pp 339−340.
(45) Stoflea, L. E.; Apostol, N. G.; Chirila, C.; Trupina, L.; Negrea, R.; Pintilie, L.; Teodorescu, C. M. Schottky Barrier versus Surface Ferroelectric Depolarization at Cu/$Pb(Zr,Ti)O_3$ Interfaces. *J. Mater. Sci.* **2014**, 10.1007/s10853-014-8041-6.
(46) Shur, V. Ya. Kinetics of Ferroelectric Domains: Application of General Approach to $LiNbO_3$ and $LiTaO_3$. *J. Mater. Sci.* **2006**, *41*, 199−210.
(47) Shur, V. Ya. In *Nucleation Theory and Applications*; Schmelzer, J. W. P., Ed.; Wiley-VCH: Weinheim, Germany, 2005; Chapter 6, pp 178−214.
(48) Sluka, T.; Tagantsev, A.; Damjanovic, D.; Gureev, M.; Setter, N. Enhanced Electromechanical Response of Ferroelectrics Due to Charged Domain Walls. *Nat. Commun.* **2012**, *3*, 748.
(49) Zubko, P.; Jung, D. J.; Scott, J. F. Space Charge Effects in Ferroelectric Thin Films. *J. Appl. Phys.* **2006**, *100*, 114112.
(50) Kaemmer, K.; Huelz, H.; Holzapfel, B.; Haessler, W.; Schultz, L. Electrode Influence on the Polarization Properties of $BaTiO_3$ Thin Films Prepared by off-Axis Laser Deposition. *J. Phys. D: Appl. Phys.* **1997**, *30*, 522−528.
(51) Jia, Z.; Ren, T. L.; Liu, T. Z.; Hu, H.; Zhang, Z. G.; Xie, D.; Liu, L. T. Comparison of Properties of Pt/PZT/Pt and Ru/PZT/Pt Ferroelectric Capacitors. *Chin. Phys. Lett.* **2006**, *23*, 1042−1045.
(52) Pintilie, L.; Dragoi, C.; Stancu, V.; Pintilie, I. The Influence of the Electrode Type on the Electric−Ferroelectric Properties of Sandwich $PbZr_{0.2}Ti_{0.8}O_3$-$BiFeO_3$-$PbZr_{0.2}Ti_{0.8}O_3$Structure. *Ferroelectrics* **2009**, *391*, 58−66.
(53) Bhaskar, S.; Majumder, S. B.; Dobal, P. S.; Krupanidhi, S. B.; Katiyar, R. S. Dielectric and Ferroelectric Response of Sol−Gel Derived $Pb_{0.85}La_{0.15}TiO_3$ Ferroelectric Thin Films on Different Bottom Electrodes. *Thin Solid Films* **2002**, *406*, 30−39.
(54) Simoes, A. Z.; Ramırez, M. A.; Longo, E.; Varela, J. A. Leakage Current Behavior of $Bi_{3.25}La_{0.75}Ti_3O_{12}$ Ferroelectric Thin Films Deposited on Different Bottom Electrodes. *Mater. Chem. Phys.* **2008**, *107*, 72−76.
(55) Noel, Y.; Zicovich-Wilson, C. M.; Civalleri, B.; D'Arco, Ph.; Dovesi, R. Polarization properties of ZnO and BeO: An Ab Initio Study through the Berry Phase and Wannier Functions Approaches. *Phys. Rev. B* **2001**, *65*, 014111.
(56) Allen, M. W.; Mendelsberg, R. J.; Reeves, R. J.; Durbin, S. M. Oxidized Noble Metal Schottky Contacts to *n*-Type ZnO. *Appl. Phys. Lett.* **2009**, *94*, 103508.
(57) Downey, B. P.; Meyer, D. J.; Katzer, D. S.; Storm, D. F.; Binari, S. C. Electrical Characterization of Schottky Contacts to N-Polar GaN. *Solid-State Electron.* **2013**, *86*, 17−21.
(58) Rychkov, D.; Gerhard, R.; Ivanov, V.; Rychkov, A. Enhanced Electret Charge Stability on Polyethylene Films Treated with Titanium-Tetrachloride Vapor. *IEEE Trans. Dielectr. Electr. Insul.* **2012**, *19*, 1305−1311.
(59) Pantel, D.; Goetze, S.; Hesse, D.; Alexe, M. Reversible Electrical Switching of Spin Polarization in Multiferroic Tunnel Junctions. *Nat. Mater.* **2012**, *11*, 289−293.
(60) Pantel, D.; Goetze, S.; Hesse, D.; Alexe, M. Room-Temperature Ferroelectric Resistive Switching in Ultrathin $Pb(Zr_{0.2}Ti_{0.8})O_3$ Films. *ACS Nano* **2011**, *5*, 6032−6038.
(61) Chanthbouala, A.; Garcia, V.; Cherifi, R. O.; Bouzehouane, K.; Fusil, F.; Moya, X.; Xavier, S.; Yamada, H.; Deranlot, C.; Mathur, N. D.; Bibes, M.; Barthélémy, A.; Grollier, J. A Ferroelectric Memristor. *Nat. Mater.* **2012**, *11*, 860−864.
(62) Hong, S.; Choi, T.; Jeon, J. H.; Kim, Y.; Lee, H.; Joo, H.-Y.; Hwang, I.; Kim, J.-S.; Kang, S-O. S.; Kalinin, V.; Park, B. H. Large Resistive Switching in Ferroelectric $BiFeO_3$ Nano-Island Based Switchable Diodes. *Adv. Mater.* **2013**, *25*, 2339−2343.
(63) Heremans, P.; Gelinck, G. H.; Muller, R.; Baeg, K.-J.; Kim, D.-Y.; Noh, Y.-Y. Polymer and Organic Nonvolatile Memory Devices. *Chem. Mater.* **2011**, *23*, 341−358.
(64) Asadi, K.; de Boer, T. G.; Blom, P. W. M.; de Leeuw, D. M. Tunable Injection Barrier in Organic Resistive Switches Based on Phase-Separated Ferroelectric−Semiconductor Blends. *Adv. Funct. Mater.* **2009**, *19* (19), 3173.